Detectability and Detection Distance Evaluation of DTBird Models

Revision: 01
Company: Liquen Consultoría Ambiental, S.L.
Project: Evaluation of Detection Distance using a drone flight
Reference: 010_D11_12_2024

VERSION HISTORY

DATE	REV.	AUTHOR(S) REVISOR(S)	DESCRIPTION
28/07/2025	00	Javier Hernández (A) Milagros Bonacchi (R)	First version of the document
04/08/2025	01	Javier Hernández (A, R)	Revision

INDEX

SUMMARY

This study objectively and replicably evaluates the detection capabilities of DTBird models (F4, A4, F6, A6, y DTBirdT – see Catalog), through controlled flights with an avian mimic drone. The data obtained allows performance expectations to be adjusted and facilitates technical decisions based on real data, in order to determine the DTBird model that best suits each wind turbine, target species, and scope of the system.

The main objective is to empirically estimate the effective detection distance of each DTBird model, as well as to model its ability to detect objects in flight as a function of distance. The experiment was carried out in a controlled environment, using a mimetic drone with a morphology similar to that of a medium-sized bird of prey as a reference object.

Specific flights were carried out following trajectories designed to cover a wide range of distances, angles of entry, and visibility conditions. These trajectories were recorded by GPS and synchronized with the video recordings from the cameras, allowing the detection distances per event to be calculated accurately.

Based on this data, the differences in detection range between the different DTBird models were analyzed. Subsequently, using theoretical flights and statistical modeling, the probability of detection was estimated as a function of the average distance to the system. To do this, Generalized Additive Models (GAMs) were used, which allowed for a flexible description of the nonlinear relationship between distance and detection rate, also incorporating the functional differences between the DTBird models.

1. INTRODUCTION

Automatic detection of birds in flight has become an essential tool in modern environmental management, particularly in sectors such as wind energy and linear infrastructure, where effective prevention of collisions with wildlife is a priority. In recent years, the growing proliferation of automatic detection systems (ADS), based on optical technologies and advanced recognition algorithms, has generated an urgent demand for objective methods to evaluate and certify their actual capabilities in operational environments.

Despite technological advances, there are currently no standardized procedures or widely accepted methodologies that allow for the accurate measurement of the actual operational performance of these systems, especially with regard to effective bird detection distances.

With this evaluation methodology, DTBird pursues the following specific objectives:

1. **Obtain the maximum and effective bird detection distances** of DTBird models using a standard flying object (avian mimic drone) under controlled conditions.
2. **Analyze and compare** the detection capabilities between different DTBird models.
3. **Evaluate the actual detection capability** of each DTBird model based on the distance to the bird, using rigorous statistical and comparative analysis.
4. **Model the probability of bird detection** based on distance for each DTBird model, thus establishing clear thresholds for effective detection.
5. **Extrapolate the results** obtained to estimate the expected detection distance for birds of different sizes and morphologies.
6. **Identify technical and methodological limitations** of the experimental design implemented, proposing practical improvements for future replicas of the study as hardware/software capabilities improve and we develop new DTBird models.

2. METHODOLOGY

The methodological flow followed in this study is summarized visually below. Each stage is described in detail in the following sections.

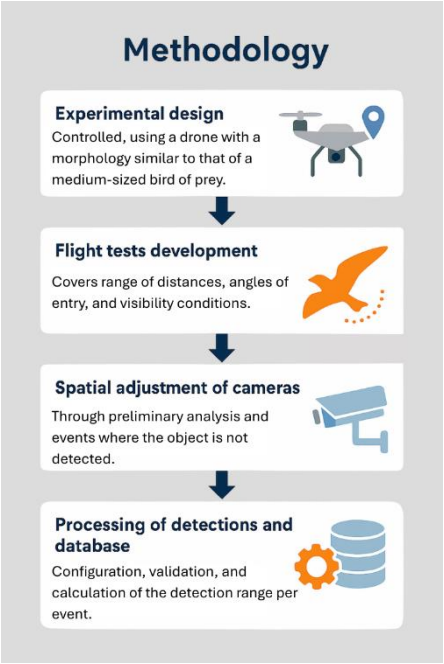

Figure 1. Visual summary of the methodology used.

2.1 Experimental design

The experiment was carried out in an open environment in the municipality of Trescasas (Segovia), at an altitude of 1,148 meters above sea level, in a location selected for its absence of visual obstacles and ease of spatial control. A mimetic drone from Ventor Innovations was used as a reference object, designed with a wingspan of 1.42 meters and a total length of 0.82 meters. This device simulates the appearance and proportions of a medium-sized bird of prey (Figure 2), allowing controlled trajectories to be reproduced for system evaluation.

The detection system was installed on an orthogonal wooden module designed to house cameras on its side faces (Figure 3). These were distributed in four positions (P1, P2, P3, and P4), oriented according to the cardinal axes. Position P1 (North) included four cameras used in the DTBird Falco (F) models used in terrestrial environments, and Albatross (A) models used in marine projects and/or with stereoscopic technology: F4/A4, F6/A6, and T models. Positions P2, P3, and P4 had two cameras each, combining F4 and A4 models.

The Albatross (A) models were configured with 60° (B079 lens) and 95° (B061 lens) lens modules, used in a 16:9 aspect ratio and with a maximum resolution of 8 MPX.

The orientation with respect to north for each position was taken in the field at the time of module placement. This orientation, subsequently validated and corrected using GIS tools, allowed the space to be structured into defined quadrants and facilitated spatial analysis in later phases.

Figure 2 (Left). Image of the Ventor mimetic drone used. **Figure 3 (Right).** Camera box used in its final location in Trescasas, Segovia.

2.2 Flight tests development

The flight tests were conducted on December 17, 2024, in the afternoon. During this day, two different flight sequences were carried out, using patterns designed to cover a wide range of distances and trajectories with respect to the detection system. The first flight (Flight 1) took place between 2:20 p.m. and 3:32 p.m., and the second (Flight 2) between 4:40 p.m. and 5:00 p.m. (GMT+1).

In the first phase (Flight 1), the drone flew in concentric circles at different distances, starting from positions far away from the camera module. In the second phase (Flight 2), trajectories in the form of circles, figure eights, and random flights were implemented to simulate non-linear approaches and evaluate the system's performance in the face of sudden changes in direction and variable angles of entry into the field of view. The set of recorded trajectories is shown in Figure 4.

The position of the drone was continuously recorded by GPS, with a sampling frequency of 10 Hz. The recorded data included latitude, longitude, and altitude in decimal format, as well as timestamps accurate to tenths of a second (UTC). Simultaneously, the ADS system cameras recorded all events in high resolution, with time coding visible in the videos.

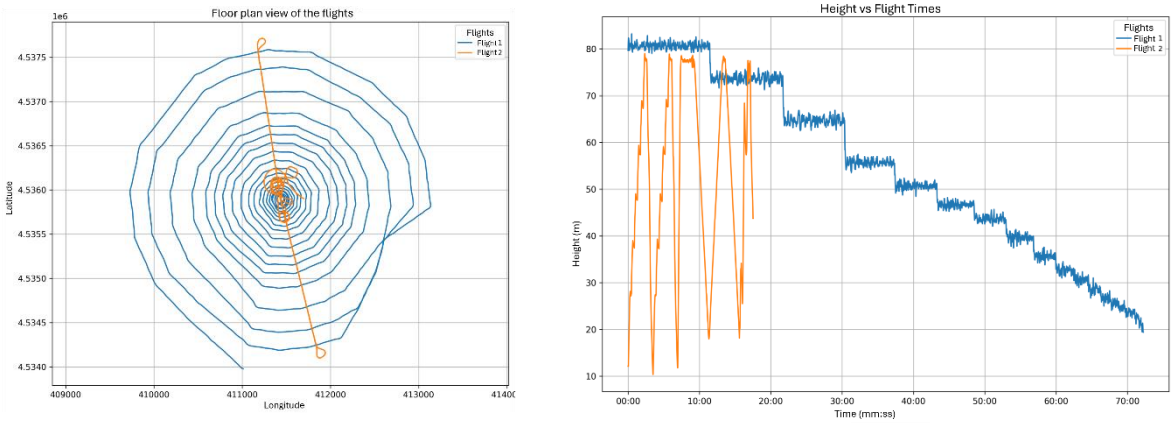

Figure 4. Drone registration for flight 1 (blue) and flight 2 (orange) in horizontal view (left, Lat/Long) and vertical view (right, Height).

Weather conditions during the experiment were stable. The day was dry, with no precipitation recorded. The maximum temperature reached 14°C and the minimum was -1°C. During the experiment, the sky remained clear, after some light high cloud cover in the early morning. Relative humidity ranged from 45% to 95%, with no significant wind. These conditions favored good visibility throughout the flights.

2.3 Preliminary analysis and spatial adjustment of models

Before beginning the analysis of the detections, a spatial and temporal validation phase of the detection system was carried out. This stage included checking the actual orientation of each device, adjusting the theoretical viewing angles, and precisely synchronizing the video recordings with the drone's GPS logs.

First, the position and orientation of each camera was verified using GIS tools. Based on the coordinates and orientations taken in situ, simulations of the theoretical fields of view of each lens were constructed using the optical specifications declared by the manufacturer. These simulations were superimposed on high-resolution orthophotos in *QGIS 3.34.15* (https://qgis.org/), allowing the expected coverage to be compared with the actual coverage. By identifying fixed elements in the landscape (buildings, road corners, plot edges, projected shadows, etc.), the bearings were manually adjusted until a precise visual correspondence was achieved between the areas visible in the videos and the simulated polygons (Figure 5). This process allowed us to correct small deviations in the initial orientation recorded in the field, which are especially relevant in cameras with narrow viewing angles (60°), where a minimal deviation can substantially modify the operational field.

At the same time, the system's time recording was validated. The cameras generated a time stamp printed on each recording, while the drone recorded its trajectory in GPS format with time stamps in UTC format and accuracy to the nearest tenth of a second. To ensure synchronization, specific sequences from the second flight were selected, where the trajectories presented easily identifiable patterns. By comparing the drone's entry/exit time in the theoretical field of view (according to GPS) with the visual time recorded on video, a small systematic offset was identified and corrected to improve accuracy.

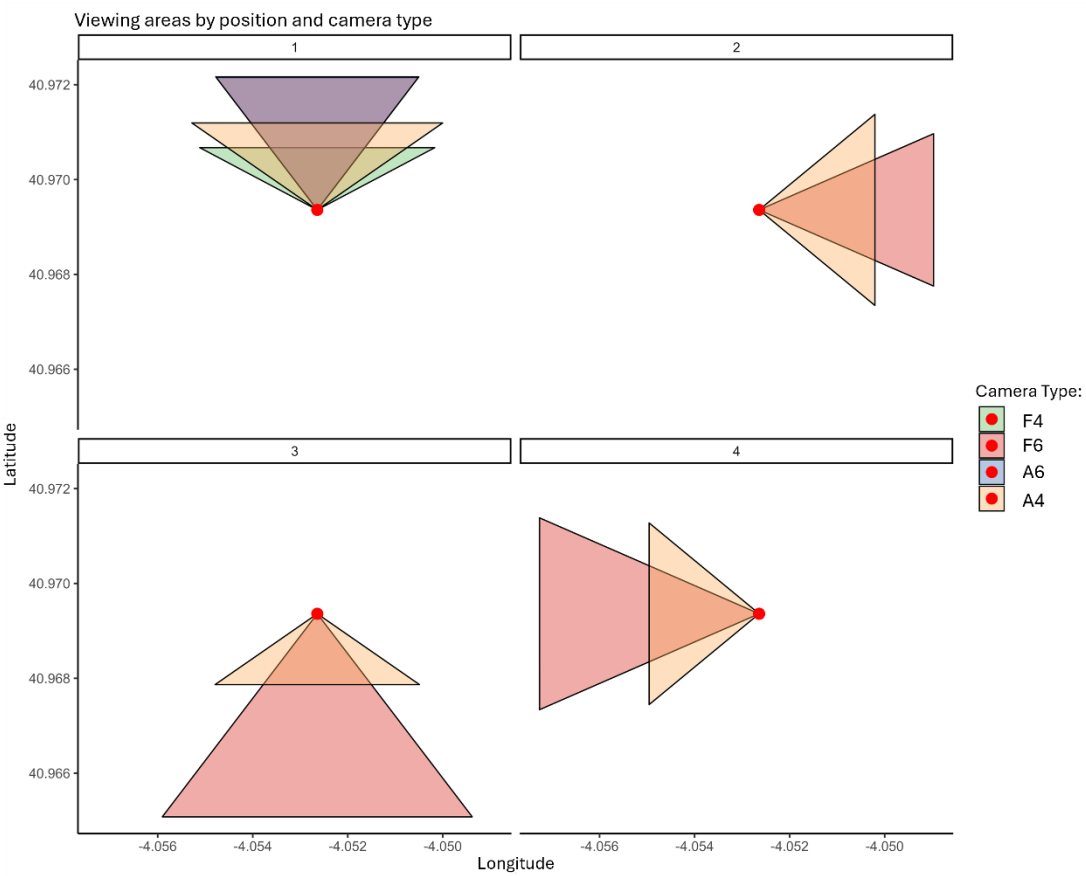

Figure 5. Theoretical representation of the fields of view of the optical cameras by position after final adjustment. Each triangle shows the simulated horizontal aperture angle for each camera installed in positions 1 to 4 of the detection module. The polygons are projected onto geographic coordinates (latitude/longitude) and colored by camera type.

2.4 Processing of detections and construction of the database

Once the spatial and temporal data had been validated, the automatic detections generated were processed in order to build a refined and structured database that would allow the actual detection distances to be quantified.

The detections were obtained from the analysis of the original recorded videos (Figure 6.). Since the automatic detection software (*Larus*®) incorporates morphological and behavioral filters, it was necessary to adjust its configuration to optimize the detection of the mimetic drone, whose trajectories tend to be more rectilinear than those of a real bird. This made it possible to increase the number of events detected without restricting the type of movement or classification of the object.

In addition, spatial validation by detection was implemented, verifying that the drone was effectively within the theoretical field of view of the corresponding camera at the time of recording. In cases where spatial inconsistencies were detected, the event was discarded.

The final result was a structured database that integrates, for each detection: unique identifier, camera model, filter settings applied, start and end times of each event, drone position, and distance metrics. This database was used both for the empirical characterization of detection distances and for the statistical modeling of the probability of detection as a function of distance.

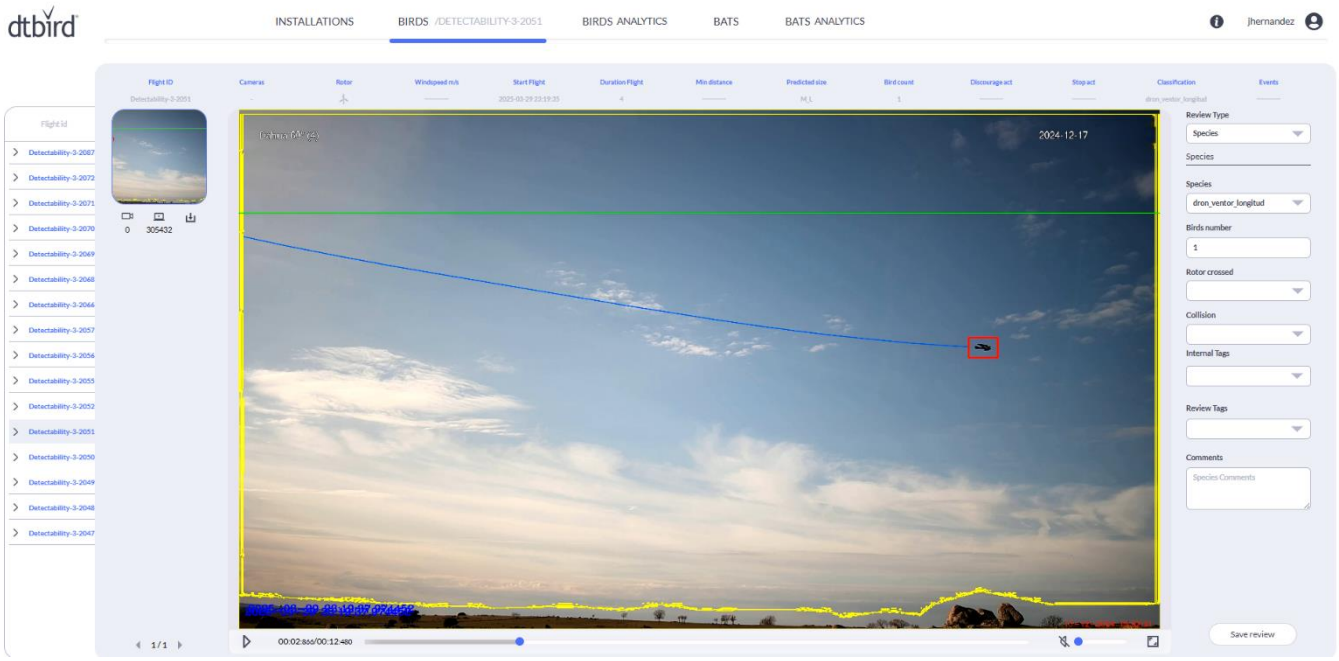

Figure 6. Visualization of a detection of the mimetic drone flight through the NEST® platform, used to review detections generated by DTBird® systems. The complete trajectory of the object (blue line), the position where it was detected (red box), and the visualization context (field of view, horizon, and associated metadata) are shown.

2.5 Estimation of maximum detection distances

The distance between the drone and the camera system was calculated in a GIS environment using *R 4.4.2* in *RStudio* (https://posit.co/) and functions from the *sf* and *geosphere* packages, taking into account the latitude, longitude, and altitude of the drone at each moment. The three-dimensional Euclidean distance between each point of the drone and the fixed location of the detection module was used, generating a distance value in meters and another in degrees for each position.

From the refined database of actual detections, the GPS positions of the drone at the beginning and end of each detection interval were extracted, previously synchronized with the video timestamp. This allowed each event to be temporally delimited and the minimum, maximum, and average distances correspond to that interval to be obtained.

For this specific analysis, only the maximum distance of each detection was used as the main variable to characterize the operational range of each type of camera/DTBird model. These values were then used in the comparative graphs by model and filter configuration.

2.6 Detectability analysis

To evaluate the relationship between distance and detection probability, theoretical flights were generated based on the intersection between the drone's GPS trajectories and the field

of view simulations of each camera in a GIS environment. Each time the drone entered and exited the theoretical field of view of a camera, an individual theoretical flight was defined, for which the average distance to the detection system during that interval was calculated.

Each theoretical flight was assigned a binary label (1 = detected, 0 = not detected) depending on whether it coincided temporally with any actual detection recorded by the corresponding camera. This coding allowed us to construct a binary database with observations per flight, containing the average distance as the main variable and the type of camera/DTBird model as an explanatory factor.

Statistical modeling was performed in R, using different approaches with binomial distribution and *logit* link function. Three main strategies were explored and compared:

- Simple logistic models: adjusted by camera, they allowed the general shape of the relationship between distance and detection probability to be evaluated but forced a sigmoid shape that did not correspond to the variability observed in some cameras.
- Segmented models (*segmented* package): logistic lines were adjusted with automatically estimated change points, allowing for the capture of possible thresholds or abrupt drops in detectability. While they offered useful interpretations (such as threshold distances), their rigidity in form and linear segmentation limited their ability to represent non-monotonic or bimodal relationships.
- Generalized Additive Models (GAMs) (*mgcv* package): distance smoothing was used to model the relationship in a flexible and non-parametric way. This strategy allowed us to capture complex patterns without imposing a specific functional form.

The choice of GAMs was based on both statistical and conceptual criteria. Firstly, the relationship between distance and detection probability was not expected to be either linear or strictly decreasing: some cameras showed peaks in detectability at medium distances, with drops at both short distances (due to shadowing or centering) and long distances. GAMs allowed these curves to be modeled naturally.

Secondly, the evaluated system included cameras with very different aperture angles used in the different DTBird models, which affects how the object projects its movement onto the frame. This effect could modify not only the detection range, but also the functional shape of the curve, especially in closed-angle cameras. A linear or segmented model could not adapt to this variability without artificially multiplying the parameters.

Finally, the database was unbalanced, with a lower proportion of flights detected compared to the total, and an uneven distribution by distance. This required models that were robust to imbalance and with complexity control, something that GAMs allowed to be adjusted through automatic smoothing penalty (*sp* parameter) and validation by AIC and EDF.

Different GAM structures were compared. The selected model incorporates smoothing differentiated by camera type, offering the best balance between fit, interpretability, and consistency with the logic of the system. This model was used as the basis for estimating detectability curves as a function of distance and camera type/DTBird model, as well as for extrapolating the results to species of different sizes according to their relative wingspan.

3. RESULTS

3.1 Maximum detection distances

As a starting point for interpreting the results, the detection distances obtained exclusively on the 1.4 m wingspan bird of prey mimic drone, used as a standard object in all flights, were analyzed. The cameras on the DTBird F6 and A6 models with smaller lens angles showed the longest detection distances, with medians close to 180 m and maximums of 451.3 m and 359.7 m, respectively (Figure 7). Conversely, as expected, the DTBird models with larger lens angles, DTBird F4 and A4, had lower mean values (~135 m) and less dispersion. In this case, the Kruskal-Wallis test reflected a trend toward significance ($\chi^2 = 7.72$, $p = 0.052$), although no statistically significant differences were reached. Pairwise comparisons using the Wilcoxon test showed no significant differences ($p > 0.05$), although the difference between A4 and F6 (adjusted $p = 0.11$) suggests a possible separation that could be confirmed with a larger sample size. These values summarize the effective performance of the system under optimal conditions and allow robust comparative ranges to be established for each device. The complete results for each DTBird camera/model, along with extrapolations by species, can be found in the Appendix.

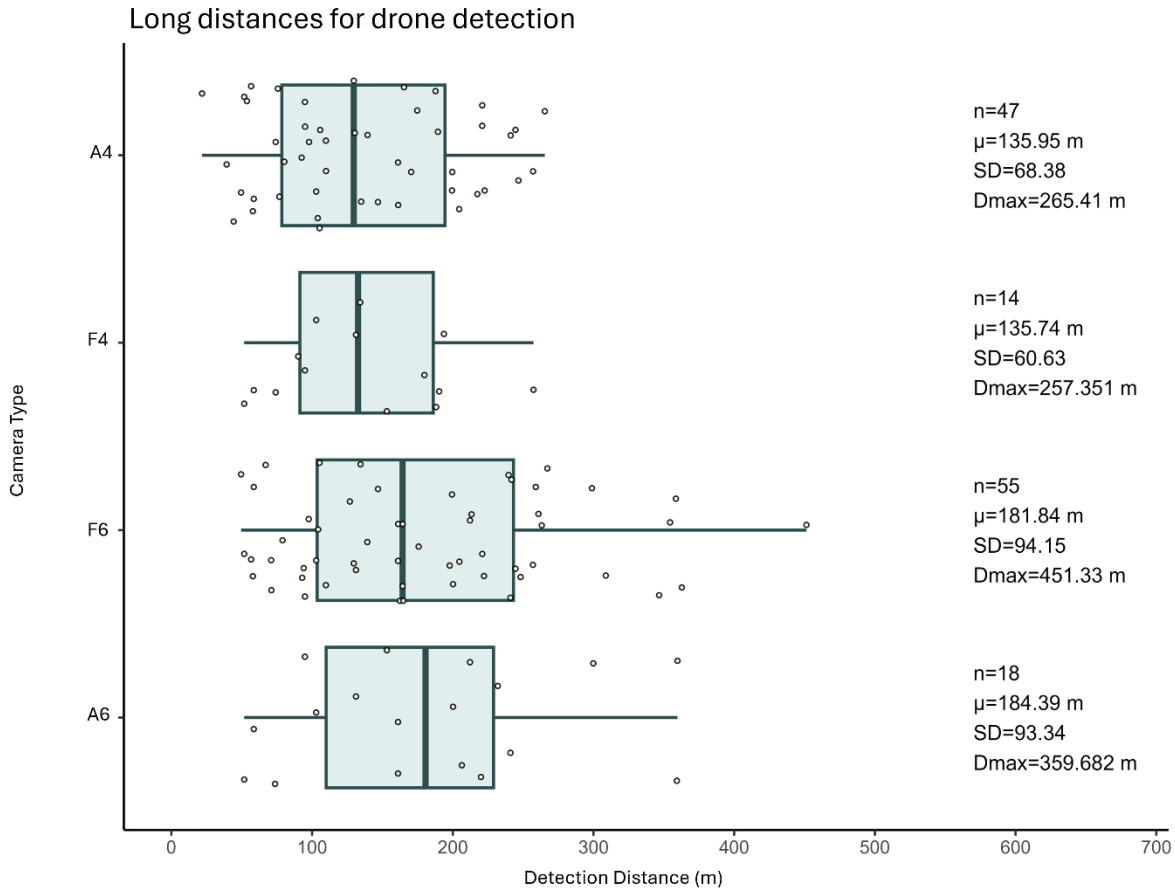

Figure 7. Boxplots of the detection distance for each type of camera without applying CNN filtering. F6 and A6 show the highest distances and greatest dispersion, while F4 and A4 are concentrated around lower average values. No statistically significant differences were detected between cameras. The drone has a wingspan of 1.42 m.

3.2 Detectability based on distance

The proportion of flights detected showed a clear dependence on distance and camera type/DTBird model. The wide-angle and standard cameras used in the DTBird models evaluated showed high detectability at short distances, with a gradual or abrupt decrease as distance increased (Figure 8). The distribution of theoretical flights (Figure 9) shows how the DTBirdF6 and A4 models accumulated a greater number of flights at medium and long distances, respectively, thus increasing the opportunities for detection at these distances.

Generalized additive models (GAM) allowed for flexible representation of the nonlinear relationship between the average distance to the drone and the detection probability for each type of camera/DTBird model (Figure 10).

The cameras on the F4 and A6 models showed sharp drops in detectability, falling from values close to 100% to practically 0% at relatively short distances (between 172 and 302 m on the F4; between 197 and 550 m on the A6).

In contrast, the F6 and A4 models showed smoother transitions, maintaining detectability above 90% at greater distances (274 m for F6 and 92 m for A4), with a gradual loss up to 619 m and 557 m, respectively.

These GAM curves confirm the patterns observed with logistic models but offer a more realistic representation of gradual transitions.

In addition, the extracted thresholds (90%, 50%, and total drop) allow for the delimitation of areas of high, medium, and low probability of detection, facilitating their operational application in the field.

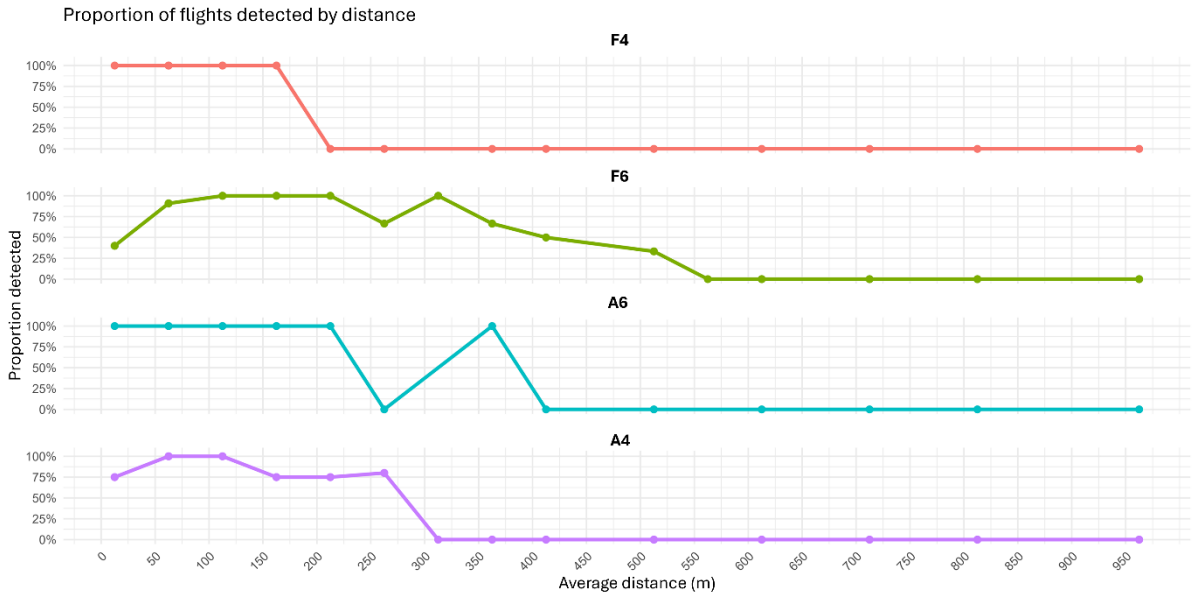

Figure 8. Proportion of flights detected in relation to average distance (in 50 m bins) for each type of camera. The colored lines show the detection rate relative to theoretical flights. A loss of detectability is observed with increasing distance, particularly pronounced in DTBird F4 and A4 models.

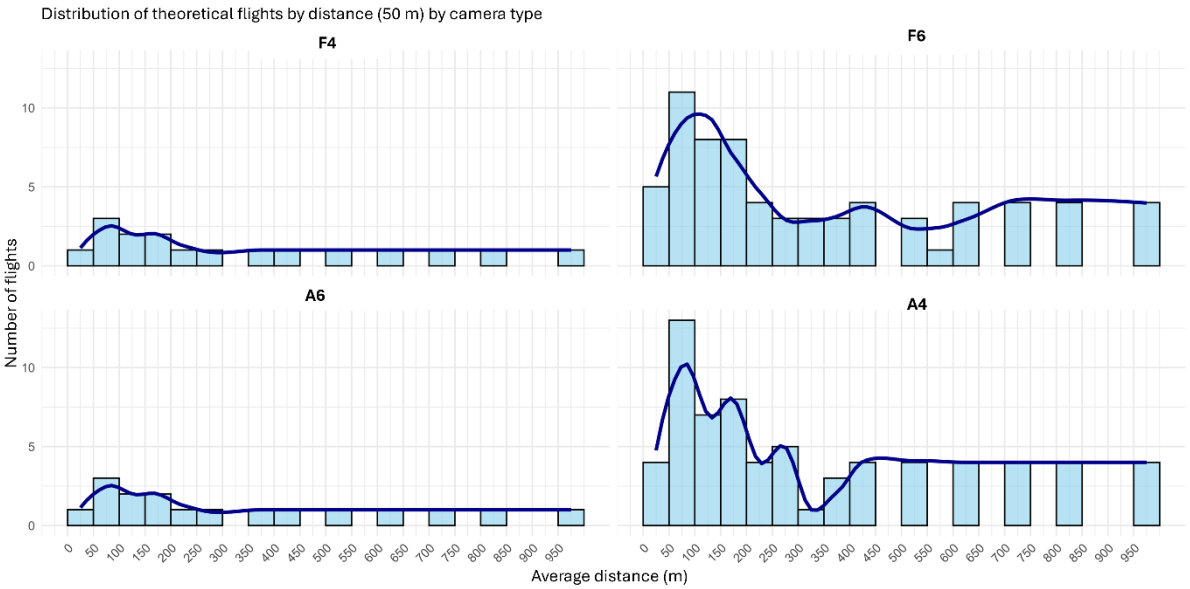

Figure 9. Distribution of theoretical flights by average distance (grouped in intervals of 50 m) for each type of camera. The blue line represents a smoothing curve to facilitate interpretation of the trend.

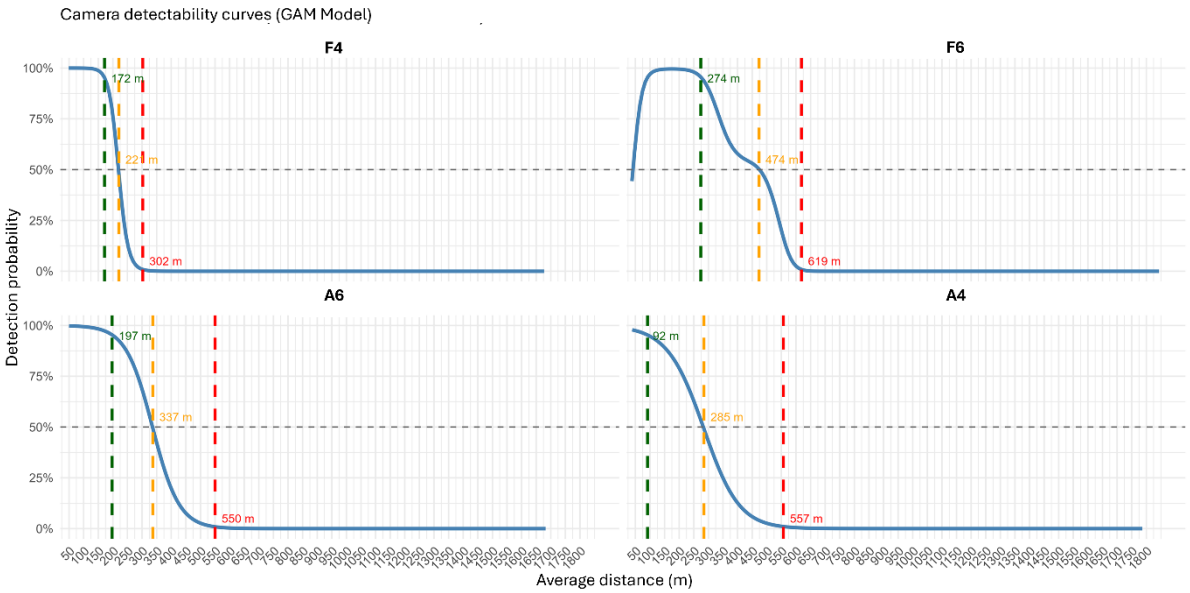

Figure 10. Detectability curves adjusted using generalized additive models (GAM) for each type of camera. The blue line represents the probability of detection as a function of the average distance to the drone. The vertical lines indicate the operational detection thresholds: green (90%), orange (50%), and red (no detection). A progressive loss of detectability with distance can be observed, more abrupt in the DTBirdF4 and A6 cameras/models, and more widespread in the DTBirdF6 and A4 cameras/models.

4. CONCLUSIONS

This report demonstrates the detection capabilities of DTBird models at different distances, providing users with transparency, verifiable data, and tools to optimize their operational deployment. The replicable and adaptive approach can be implemented in new DTBird models, providing a solid foundation for calibration and evaluation under real field conditions.

The results are consistent with independent evaluations of the detection capabilities of older DTBird models and obsolete software versions. See document: 2° Evaluation Phase of DTBird System V4D8. May 2024.

Limitations

The results of the study have a number of limitations that should be taken into account.:

- Controlled conditions: The experiment was conducted in a clear environment, without visual obstacles, under stable weather conditions and clear skies. These factors do not fully reflect actual operating conditions, where different weather/lighting and contrast conditions and potential visual obstacles alternate.
- Single reference object: The use of a 1.4 m mimetic drone shaped like a bird of prey provides experimental consistency, but does not allow for the capture of morphological, color, or behavioral variability among different bird species.
- Relationship with real species: Extrapolation by wingspan is a useful but simplified approximation, as it does not take into account other relevant variables such as visual contrast, wing flapping, speed, or direction of entry into the field of view, all of which can affect the probability of detection. Therefore, the results derived from extrapolation to species with morphology, size, or flight behavior very different from that of the drone should be understood as indicative and should be interpreted with caution and technical judgment.
- Limitation of drone use: The *Larus*® configuration is *designed to eliminate* non-bird flying objects, so the configuration had to be adapted to match the detectability of drones with that of birds.
- Certain imbalances were identified in flight density at intermediate distances, as well as in the angular coverage of some cameras. These asymmetries can affect both the stability of the adjusted models and the informativeness of the descriptive metrics, particularly the mean, which is more sensitive to non-homogeneous distributions.

dtbird dtbat
AUTOMATIC & REAL-TIME PROTECTION

Appendices

APPENDIX A

DESCRIPTIVE METRICS OF MAXIMUM DETECTION DISTANCES: DTBIRDF6

Table 1A. Maximum detection distances extrapolated by species for the DTBirdF6 camera/model. The values shown are the mean distance, standard deviation, absolute maximum, maximum confidence interval, and median. The values are estimated from the data collected by the mimic drone using a scale factor proportional to the wingspan of each species. In the case of the drone, the number of valid detections is also indicated.

F6			N	Mean	SD	Absolute max.	Median
Species	**Wingspan (m)**	**Cat.**					
Black Vulture	2,95	Large	--	377,76	195,6	937,62	341,46
Griffon Vulture	2,6	Large	--	332,94	172,39	826,38	300,95
Golden Eagle	2,2	Large	--	281,72	145,87	699,24	254,65
Egyptian Vulture	1,7	Medium	--	217,69	112,72	540,32	196,77
Red Kite	1,55	Medium	--	198,48	102,77	492,65	179,41
Drone	**1,42**	**Medium**	**55**	**181,84**	**94,15**	**451,33**	**164,36**
Lesser Kestrel	0,73	Small	--	93,48	48,4	232,02	84,5

APPENDIX B

DESCRIPTIVE METRICS OF MAXIMUM DETECTION DISTANCES: DTBIRDF4

Table 1B. Maximum detection distances extrapolated by species for DTBirdF4 cameras/models. The values shown are the mean distance, standard deviation, absolute maximum, maximum confidence interval, and median. The estimates are based on the behavior of the bird-shaped drone with a wingspan of 1.4 m and are scaled proportionally according to the wingspan of each species.

F4			N	Mean	SD	Absolute max.	Median
Species	**Wingspan (m)**	**Cat.**					
Black Vulture	2,95	Large	--	282	60,63	534,64	275,65
Griffon Vulture	2,6	Large	--	248,54	111	471,21	242,94
Golden Eagle	2,2	Large	--	210,3	125,95	398,71	205,57
Egyptian Vulture	1,7	Medium	--	162,51	93,93	308,1	158,85
Red Kite	1,55	Medium	--	148,17	85,39	280,91	144,83
Drone	**1,42**	**Medium**	**14**	**135,74**	**66,18**	**257,35**	**132,69**
Lesser Kestrel	0,73	Small	--	69,78	31,17	132,3	68,21

APPENDIX C

DESCRIPTIVE METRICS OF MAXIMUM DETECTION DISTANCES: A6

Table 1C. Maximum detection distances extrapolated by species for the DTBirdA6 camera/model with a 60° lens. The metrics presented are mean distance, standard deviation, absolute maximum, maximum confidence interval, and median. The estimates are generated from the detections of the mimic drone, scaled according to the wingspan of each species.

A6			N	Mean	SD	Absolute max.	Median
Species	**Wingspan (m)**	**Cat.**					
Black Vulture	2,95	Large	--	383,05	193,9	747,23	375,27
Griffon Vulture	2,6	Large	--	337,61	170,9	658,57	330,74
Golden Eagle	2,2	Large	--	285,67	144,6	557,25	279,86
Egyptian Vulture	1,7	Medium	--	220,74	111,74	430,61	216,25
Red Kite	1,55	Medium	--	201,27	101,88	392,61	197,17
Drone	**1,42**	**Medium**	**18**	**184,39**	**93,34**	**359,68**	**180,64**
Lesser Kestrel	0,73	Small	--	94,79	47,98	184,91	92,86

APPENDIX D

DESCRIPTIVE METRICS OF MAXIMUM DETECTION DISTANCES: A4

Table 1D. Maximum detection distances extrapolated by species for the DTBirdA6 camera/model with a 60° lens. The metrics presented are mean distance, standard deviation, absolute maximum, maximum confidence interval, and median. The estimates are generated from the detections of the mimic drone, scaled according to the wingspan of each species.

A4			N	Mean	SD	Absolute max.	Median
Species	**Wingspan (m)**	**Cat.**					
Black Vulture	2,95	Large	--	282,44	142,05	551,38	269,29
Griffon Vulture	2,6	Large	--	248,93	125,2	485,96	237,34
Golden Eagle	2,2	Large	--	210,63	105,93	411,2	200,82
Egyptian Vulture	1,7	Medium	--	162,76	81,86	317,74	155,18
Red Kite	1,55	Medium	--	148,4	74,64	289,71	141,49
Drone	**1,42**	**Medium**	**47**	**135,95**	**68,38**	**265,41**	**129,62**
Lesser Kestrel	0,73	Small	--	69,89	35,15	136,44	66,64